JACS
JOURNAL OF THE AMERICAN CHEMICAL SOCIETY

Article

pubs.acs.org/JACS

A Metal–Organic Tetrahedron as a Redox Vehicle to Encapsulate Organic Dyes for Photocatalytic Proton Reduction

Xu Jing, Cheng He, Yang Yang, and Chunying Duan*

State Key Laboratory of Fine Chemicals, Dalian University of Technology, Dalian 116024, China

Supporting Information

ABSTRACT: The design of artificial systems that mimic highly evolved and finely tuned natural photosynthetic systems is a subject of intensive research. We report herein a new approach to constructing supramolecular systems for the photocatalytic generation of hydrogen from water by encapsulating an organic dye molecule into the pocket of a redox-active metal–organic polyhedron. The assembled neutral Co_4L_4 tetrahedron consists of four ligands and four cobalt ions that connect together in alternating fashion. The cobalt ions are coordinated by three thiosemicarbazone NS chelators and exhibit a redox potential suitable for electrochemical proton reduction. The close proximity between the redox site and the photosensitizer encapsulated in the pocket enables photoinduced electron transfer from the excited state of the photosensitizer to the cobalt-based catalytic sites via a powerful pseudo-intramolecular pathway. The modified supramolecular system exhibits TON values comparable to the highest values reported for related cobalt/fluorescein systems. Control experiments based on a smaller tetrahedral analogue of the vehicle with a filled pocket and a mononuclear compound resembling the cobalt corner of the tetrahedron suggest an enzymatic dynamics behavior. The new, well-elucidated reaction pathways and the increased molarity of the reaction within the confined space render these supramolecular systems superior to other relevant systems.

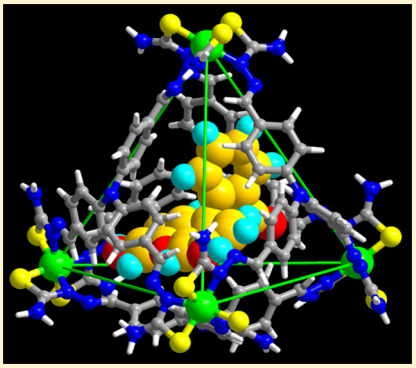

1. INTRODUCTION

The design of artificial catalysts that can compete with the catalytic proficiency of enzymes is a subject of intensive research.[1,2] The conventional route to fabricating an effective artificial enzyme is to reproduce the sometimes elusive structure of the enzyme's active site.[3,4] Recently reported models have also been designed according to the idea of enhancing the reaction rate by increasing the concentration of a substrate around its reactive center.[5,6] Accordingly, self-assembly reaction vessels based on reversible interactions have been considered a new phase of matter, in which the physicochemical properties of the molecules contained in the "molecular flask" are considerably modified with respect to those exhibited in the solid, liquid, or gas phase.[7] New reaction pathways have emerged for such substrate molecules inside these containers, by enhancing the proximity between of the substrate and the catalytic center and increasing the effective molarity of the reaction.[8,9]

Inspired by the significant advances and exciting results,[10,11] we considered whether a supramolecular strategy could provide ways of mimicking the highly evolved and finely tuned natural systems for photocatalytic water splitting,[12,13] which is an important process both in living systems and in solar energy conversion.[14,15] The essential components of artificial homogeneous systems for hydrogen evolution always involve a photosensitizer for light absorption, a catalyst for proton reduction, and an electron donor.[16] The intrinsic difficulties of mimicking natural systems thus include the feasibility of the processes occurring in aqueous solution and the presence of a well-defined pocket to force the proton reduction center and photosensitizer into close proximity.[17,18] Most importantly, to construct highly efficient and easily operated systems for photocatalytic hydrogen evolution from water, the supramolecular vessels should be designed such that at least one of the two essential components exhibit redox activity and/or light-harvesting ability.[19,20]

The supramolecular assembly of predesigned inorganic and organic building blocks is an excellent tool for constructing well-defined, nanosized molecular vessels that catalyze special chemical transformations.[21−28] Inspired by the pocket feature of natural enzymes, researchers have developed functional coordination polyhedra with various structures and catalytic activities to establish the magnificent catalysis of natural enzymes.[28−34] By incorporating three thiosemi-carbazone (**TSC**) bidentate chelators with potential guest-accessible sites into the tripod ligand backbone, we developed a new approach to assemble metal–organic polyhedra that act as a supramolecular host and redox catalyst for the photocatalytic generation of hydrogen from water (Scheme 1). The strong coordinating ability of the NS chelators was expected to enhance the stability of the molecular polyhedron and to afford cobalt ions with redox potentials suitable for proton reduction.[35,36] The pocket of the polyhedron was well-defined

Received: January 25, 2015
Published: March 4, 2015

DOI: 10.1021/jacs.5b00832
J. Am. Chem. Soc. 2015, 137, 3967−3974

Scheme 1. Procedure for the Synthesis of the Molecular Tetrahedron and Construction of the Artificial Supramolecular System for Photocatalytic Proton Reduction

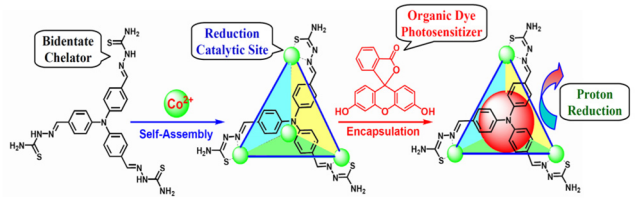

to encapsulate organic dye molecules for the construction of supramolecular photocatalytic systems. The proximity between the redox catalytic sites and the photosensitizer was expected to be enforced, and the odds of unwanted electron-transfer reactions were reduced.[37,38] The modified supramolecular system was significantly superior to systems based on a mononuclear cobalt compound resembling the cobalt corner of the polyhedron or on a smaller tetrahedral analogue with an almost solid sphere for the light-driven generation of hydrogen from water.

2. RESULTS AND DISCUSSION

The H_3**TFT** ligand, 2,2′,2″-((nitrilotris(benzene-4,1-diyl)) tris(methanylylidene))tris(hydrazinecarbothioamide), was prepared by the reaction of tris(4-formylphenyl)amine with thiosemicarbazide in a 1:3 mol ratio. The reaction of H_3**TFT** with $Co(CH_3COO)_2{\cdot}4H_2O$ in a DMF solution yielded 48% of the molecular tetrahedron Co-**TFT**. Elemental and powder X-ray analyses indicated that the bulk sample consisted of a pure phase. Magnetic susceptibility measurements suggested a diamagnetic behavior of the bulk sample, demonstrating the presence of only Co^{III} ions in the Co-**TFT** polyhedron.

The bonding of the ligands to the metal ions was also confirmed by the splitting and shifting of the resonance signals in the ^{1}H NMR spectrum of Co-**TFT** (Figure 1). Specifically,

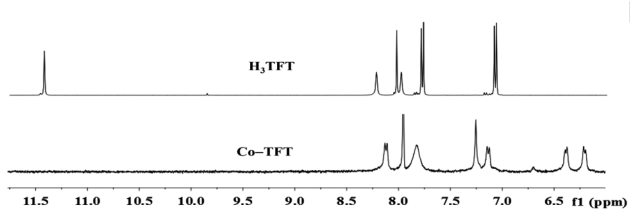

Figure 1. Partial ^{1}H NMR spectra of the free ligand H_3**TFT** (top picture) and the molecular tetrahedron Co-**TFT** (bottom picture), showing the disappearance of the imine proton C(S)−NH signals and the splitting of the phenyl ring signals upon the coordination. The peak at 7.92 ppm of the spectrum o f the complex Co-**TFT** is assignable to the protons of the DMF molecules.

the disappearance of the imine proton C(S)−NH signals at 11.38 ppm in the free ligand H_3**TFT** and the significant upfield shifts of the NH_2 protons from 8.15 and 7.91 ppm in the thiosemi-carbazone moiety of the free ligand to one peak at 7.86 ppm in the spectrum of the complex Co-**TFT** suggest that the bidentate moiety was coordinated to the metal ion. The splitting of the phenyl ring signals at 7.76 and 7.06 ppm of the ligand to 7.26 and 7.17 and 6.38 and 6.22 ppm, respectively, is also an indicator of the formation of polyhedral species; this splitting represents the significantly different chemical shifts of the protons inside and outside the polyhedron.

Single-crystal analysis clearly showed the formation of a neutral Co_4L_4 tetrahedron with an ideal C_3 symmetry via the connection of four deprotonated ligands and four cobalt ions in an alternating fashion (Figure 2). Each cobalt ion is

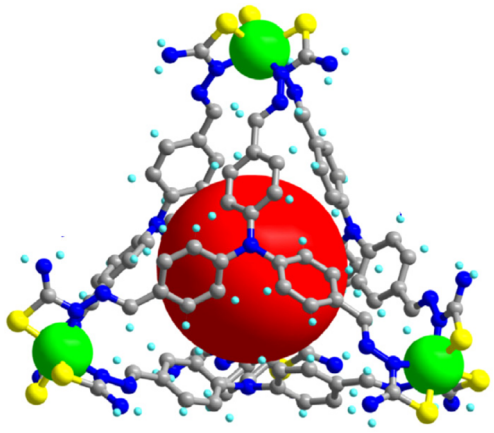

Figure 2. Structure of the molecular tetrahedron Co-**TFT**, showing the coordination geometries of the cobalt ions and the empty sphere (red ball) for the encapsulation of an organic dye, e.g., a fluorescein molecule, respectively. The cobalt, sulfur, nitrogen, and carbon atoms are drawn in green, yellow, blue, and gray, respectively.

coordinated in a *fac*-configuration by three bidentate NS chelators from three different ligands. The three anionic sulfur donors are positioned on one side and hold great potential for the attachment of a proton via hydrogen-bonding interactions, thus shortening the distance between the redox sites and the proton to be reduced. The average Co−S and Co−N bond distances of approximately 2.30 and 1.96 Å, respectively, are in good agreement with those of the related Co^{III} thiosemi-carbazone complexes.[39,40] The absence of any counterions implies that the C═S and C−N(H) bonds were all transformed to C−S and C═N bonds, respectively, via loss of the imine protons during the coordination of the metal ions. The measured C−S, C−N, and N−N bond distances (Supporting Information Figures S1−S3) are all in the normal range of single- and double-bond lengths, suggesting extensive electron delocalization over the entire ligand skeleton.[41,42] In this case, the structure provides a conventional proton-transfer path within the thiolate/thioamide tautomeric equilibrium in the ligand backbone. The proton would be easily transferred onto a suitable position during the proton reduction process.[43,44] These metal thiosemicarbazone (**TSC**) complexes are therefore promising candidates for proton reduction catalysts.[45−48]

Importantly, the separation between the cobalt ions in the tetrahedron was measured to be 15.58 Å, and the average separation between two tertiary amine N atoms was measured to be 11.36 Å. The inner volume of the pocket within the Co-**TFT** tetrahedron was calculated as approximately 520 $Å^3$, and the rhombus opening exhibited two diagonal lengths of approximately 15.6 and 10.1 Å. The structural feature of the molecular tetrahedron most likely allows the encapsulation of one fluorescein (**Fl**) molecule in its pocket, producing an artificial supramolecular system for the light-driven generation of hydrogen from water.

DOI: 10.1021/jacs.5b00832
J. Am. Chem. Soc. 2015, 137, 3967−3974

The ESI-MS spectrum of compound Co-**TFT** in the solution exhibits an intense peak at m/z = 2417.19 that is assigned to the single charged $[Co_4(\mathbf{TFT})_4]^-$ species, suggesting the formation and stability of the M_4L_4 species in solution. When an equimolar amount of fluorescein **Fl** was added into the solution of Co-**TFT**, a new intense peak at m/z = 2749.23 was observed. A simple comparison with the simulation results based on natural isotopic abundances suggests that the peak is properly assigned to a $[\mathbf{Fl} + Co_4(\mathbf{TFT})_4]^-$ species (Figure 3). This result implies the formation of a 1:1 stoichiometric complexation species $\mathbf{Fl} \subset Co_4(\mathbf{TFT})_4$ in the solution.

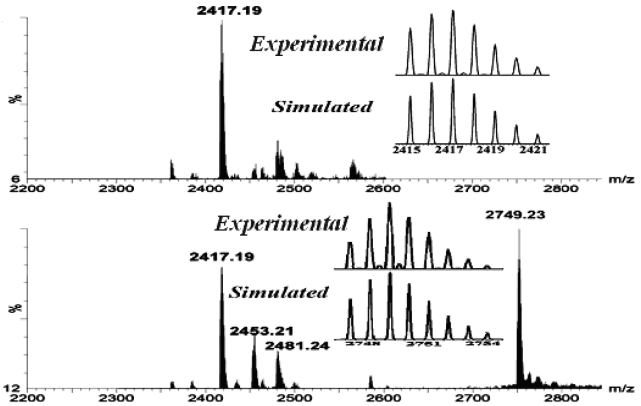

Figure 3. ESI-MS spectra of Co-**TFT** in a methanol/acetonitrile solution (top picture) and of **Fl** in the aforementioned solution (bottom picture). The inserts show the measured and simulated isotopic patterns at m/z = 2417.19 (top) and 2749.23 (bottom), respectively.

The ^{1}H NMR spectrum of Co-**TFT** (0.1 mM) in the presence of an equimolar amount of **Fl** shows significant upfield shifts of the signals associated with protons $H_{3,6}$ (δ = 0.15 ppm) and of other signals; these shifts provide an indicator[39] for the encapsulation of a molecule of **Fl** within the π-electron-rich pocket of the Co-**TFT** tetrahedron to give the complexation species $\mathbf{Fl} \subset Co_4(\mathbf{TFT})_4$. The NOESY spectrum of the solution of Co-**TFT** (0.1 mM) and fluorescein **Fl** (0.3 mM) shows obvious H−H interactions between the phenyl rings of **Fl** (H_c) and the tetrahedron (H_4, blue cycles) and between the phenyl rings of **Fl** (H_d) and the tetrahedron (H_3, green cycles) (Figure 4). These results demonstrate the potential $\pi-\pi$ interactions between the phenyl ring of **Fl** and the phenyl ring of the molecular tetrahedron, further confirming that the host−guest supramolecular system was stabilized by specific noncovalent interactions rather than by nonspecific static interactions.

Cyclic voltammetry of the molecular tetrahedron Co-**TFT** (1.0 mM) recorded in a DMF solution shows the coupled Co^{II}/Co^{I} and Co^{III}/Co^{II} reduction process (at approximately −1.02 V and as a shoulder at approximately −0.78 V (vs. Ag/AgCl), respectively, Figure 5a).[50] The Co^{II}/Co^{I} potential falls well within the range of that of proton reduction in aqueous media,[51] indicating that the Co-**TFT** complex in its reduced state is capable of directly reducing protons. The molecular tetrahedron Co-**TFT** is also demonstrated to be an efficient quencher of the excited state of **Fl**. The addition of 10 μM Co-**TFT** to the solution of **Fl** (10 μM) in an EtOH/H_2O solution (1:1 in volume and pH = 11.6, ensuring the same pH condition as that of the reaction mixture mentioned below for photocatalytic hydrogen evolution) quenched approximately 60% of the emission intensity of **Fl** (Figure 5b). Because the

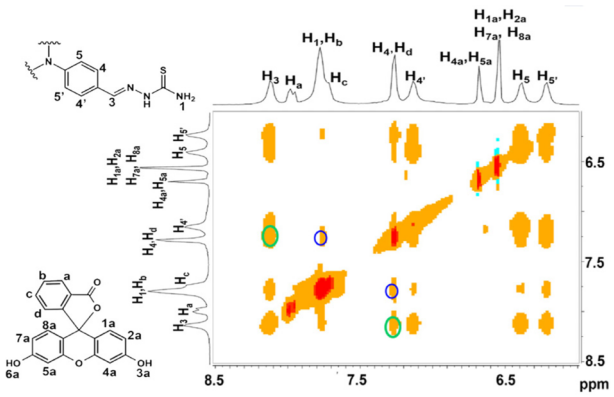

Figure 4. Partial NOESY spectrum of the Co-**TFT** (0.1 mM) and **Fl** (0.3 mM) mixture in DMSO-d_6, showing the potential interactions between the protons of the phenyl ring of the fluorescein (H_C) and the tetrahedral cage (H_4) (blue circles) and those between the protons of the phenyl rings of the fluorescein (H_D) and the molecular tetrahedron (H_3) (green circles).

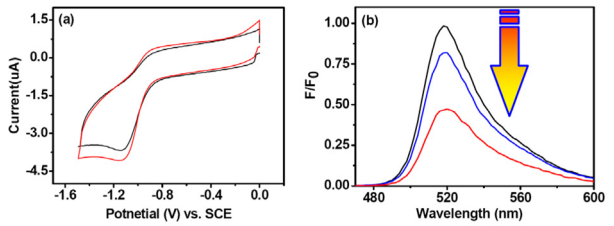

Figure 5. (a) Cyclic voltammogram of 0.1 mM Co-**TFT** (black line) and Co-**TCT** (red line), which is a smaller analogue of Co-**TFT** with an almost solid sphere, in CH_3CN containing 0.1 M $TBAPF_6$. Scan Rate: 100 mV/s. (b) Normalized fluorescence of **Fl** (10 μM, black line) in an EtOH/H_2O solution (1:1, pH = 11.6) and of the aforementioned solution upon addition of Co-**TFT**(10 μM, red line) or Co-**TCT** (10 μM, blue line).

addition of Co-**TFT** (0.1 mM) to the solution of **Fl** (0.1 mM) in EtOH/H_2O solution (1:1 in volume, pH = 11.6) did not cause any obvious changes in the absorption spectra, the quenching process is likely attributable to a classical photo-induced electron transfer (PET) from the excited state **Fl*** to the redox catalyst Co-**TFT**.[52] As a consequence, Co-**TFT** was directly activated for proton reduction by the excited state **Fl*** during irradiation and the encapsulation of fluorescein within the pocket of the tetrahedron would be a powerful method of establishing new homogeneous systems for photocatalytic hydrogen evolution.

The luminescence at 525 nm of a **Fl** solution (10 μM) containing Co-**TFT** (50 μM) decayed in a clearly exponential fashion with the lifetime, similar to the luminescence of a solution of free **Fl** (4.50 ns, Supporting Information Figure S10). Two luminescent species apparently coexisted in the titration mixture. One is the **Fl** species itself with its fluorescent lifetime being maintained; the other is the host−guest complexation species $\mathbf{Fl} \subset$ Co-**TFT**. The fact that the decay behavior approximates well to a typical single-exponential function suggests that the host−guest complexation species $\mathbf{Fl} \subset$ Co-**TFT** exhibits ignored luminescence. Upon addition of up to 50 μM Co-**TFT**, the luminescent titration profile of **Fl** (10 μM) in the solution was consistent with the Hill plot,[53] and the best fit of the titration profile suggested a 1:1 host−guest behavior with an association constant calculated as 3.38

DOI: 10.1021/jacs.5b00832
J. Am. Chem. Soc. 2015, 137, 3967−3974

($\pm$0.18) $\times$ 10^4 M^{-1} (Supporting Information Figure S12). The encapsulation of **Fl** inside the pocket of Co-**TFT** likely facilitated the PET via a fast pseudo-intramolecular pathway,[54] where the unwanted energy- and electron-transfer processes could potentially be avoided.

The irradiation of a solution containing **Fl** (2.0 mM), Co-**TFT** (4.0 μM), and triethylamine (**NEt$_3$**) (10% v:v) in a H_2O/EtOH (1:1 in volume) solution at 25 °C resulted in direct hydrogen generation.[55] A higher efficiency of hydrogen production was achieved at pH = 11.0−12.0 (Supporting Information Figure S15). Basic conditions thermodynamically favor water oxidation and facilitate further hydrogen evolution; with water replacing the sacrificial electron donors.[56] Control experiments revealed that the absence of any of these individual components led to failure to produce hydrogen, thus demonstrating that all three species are essential for hydrogen generation. Of course, the artificial system could not function well in the absence of light.

When the concentrations of **Fl** (2.0 mM) and **NEt$_3$** (10% in volume) were fixed, the volume of the hydrogen produced exhibited a linear relationship with the concentration of the Co-**TFT** catalyst in the range from 2.0 to 12.0 μM (Figure 6a). The

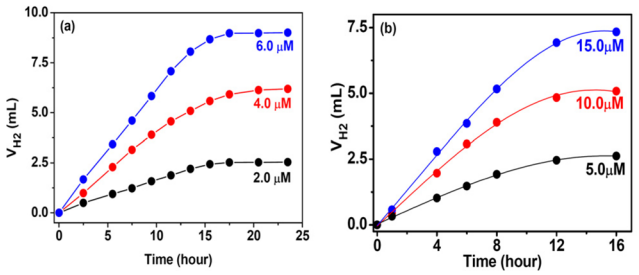

Figure 6. Light-driven hydrogen evolution of (a) the systems containing **Fl** (2.0 mM), **NEt$_3$** (10% v/v), and Co-**TFT** in an EtOH/H_2O solution (1:1, pH = 11.6) with the concentration of Co-**TFT** fixed at 2.0 μM (black), 4.0 μM (red line), and 6.0 μM (blue line); and (b) of the systems containing **Fl** (2.0 mM), **NEt$_3$** (10% v/v), and Co-**TCT** in an EtOH/H_2O solution (1:1, pH = 11.6) with the concentration of Co-**TCT** fixed at 5.0 μM (black), 10.0 μM (red line), and 15.0 μM (blue line).

initial turnover frequency (TOF) was approximately 750 mol of hydrogen per mole of catalyst per hour, and the calculated turnover number (TON) was approximately 11,000 mol of hydrogen per mole of catalyst. These values are comparable to the highest values reported for related cobalt/fluorescein systems,[35−38] demonstrating the potential advantage of the supramolecular system in photocatalytic hydrogen production from water. When the concentration of **Fl** was varied, the TOF and TON increased until a plateau value was reached at a concentration of 2.0 mM. Beyond this plateau value, the further addition of **Fl** caused little TON enhancement relevant to the Co-**TFT** catalyst. The volume of hydrogen produced was apparently not dependent on the concentration of **Fl** in the solution but was dominated by the concentration of **Fl** encapsulated inside the pocket of the molecular tetrahedron Co-**TFT**.

From a mechanistic viewpoint, the encapsulation of one molecule of the organic dye **Fl** inside the pocket of the molecular tetrahedron Co-**TFT** first enforces the proximity between the cobalt-based redox catalytic site and the photosensitizer **Fl**. This supramolecular structure then allows a direct PET process from the excited state **Fl*** to the redox catalyst.[47] Simultaneously, the close proximity between the redox site and the photosensitizer within the confined space further allows the PET to occur in a more powerful pseudo-intramolecular pathway to avoid unwanted electron transfer.

To further determine whether the photocatalytic hydrogen evolution occurred inside the pocket of Co-**TFT** through a typical enzymatic fashion or outside of the pocket in a normal homogeneous manner, an inhibition experiment was carried out by adding a nonreactive species, adenosine triphosphate (ATP), into the reaction mixture.[58] As shown in Figure 7, the

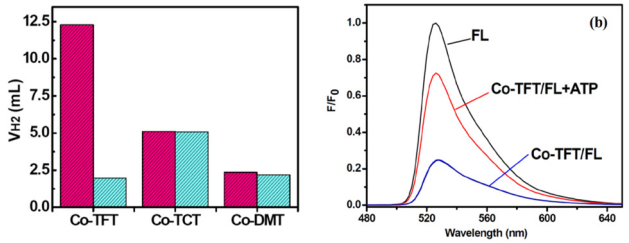

Figure 7. (a) Volume of hydrogen produced by systems containing **Fl** (2.0 mM), **NEt$_3$** (10% v/v), and redox catalysts (red bars) in EtOH/H_2O (1:1 in v:v, pH = 11.6): Co-**TFT** (10.0 μM), Co-**TCT** (10.0 μM), and Co-**DMT** (40.0 μM); the cyan bars show the aforementioned systems in the presence of ATP(2.0 mM). (b) Fluorescence spectra of **Fl**(10 μM) in EtOH/H_2O (1:1 in volume, pH = 11.6) upon addition of 0.5 mM ATP (black line), of the solution upon addition of Co-**TFT** (50 μM, blue line), and of the solution upon addition of both Co-**TFT** (50 μM) and 0.5 mM ATP (red line); the spectra show the recovery of emission in the presence of ATP when excited at 470 nm.

addition of 2.0 mM ATP efficiently quenched the photocatalytic hydrogen production by the **Fl** (2.0 mM)/ Co-**TFT** (10.0 μM)/**NEt$_3$** (10%) system. The TON value of the hydrogen produced in the presence of ATP(2.0 mM) was only 18% of the original **Fl**/Co-**TFT**/**NEt$_3$** system under the same experimental conditions. The photocatalytic reaction exhibited a competitive inhibition behavior, which means that the reaction occurred within the pocket of the molecular tetrahedron Co-**TFT**.[49] Notably, the addition of ATP (0.5 mM) to the solution mixture containing **Fl** (10 μM) and Co-**TFT** (50 μM) resulted in an emission recovery of the same band. The addition of ATP (0.5 mM) to the solution of **Fl** (10 μM) did not cause any quenching of the emission of **Fl** (Figure 7b, dark line). The recovery of the emission of **Fl** confirmed the substitution of the encapsulated **Fl** molecules in the pocket of the molecular tetrahedron Co-**TFT** by ATP molecules.

Interestingly, the addition of ATP (0.4 mM) to a solution of the molecular tetrahedron Co-**TFT**(0.1 mM) caused obvious upfield shifts of the aromatic protons relevant to the adenosine ring and a significant splitting of the signals relevant to the trisphenylamine protons in Co-**TFT** (Supporting Information Figure S8). Apparently, $\pi\cdots\pi$ stacking interactions occurred between the adenosine ring of ATP and the benzene rings of the molecular tetrahedron Co-**TFT**, providing an indicator for the encapsulation of ATP molecules in the pocket of the tetrahedron. Meanwhile, Co-**TFT** (10 μM) in a DMF solution exhibited a weak emission band centered at 450 nm when excited at 370 nm. Upon addition of up to 0.2 mM ATP into the aforementioned solution, an emission enhancement of this band of up to 210% was observed. The Hill plot of the titration profile suggests a 1:1 host−guest behavior, with an association constant for the ATP ⊂ Co-**TFT** inclusion species calculated as

DOI: 10.1021/jacs.5b00832
J. Am. Chem. Soc. 2015, 137, 3967−3974

$1.66 \pm 0.12 \times 10^5\ M^{-1}$ (Supporting Information Figure S11). This value is approximately 5 times larger than that of the **Fl** ⊂ Co-**TFT** inclusion species, suggesting the possibility of ATP molecules substituting the encapsulated **Fl** molecules and occupying the pocket of the molecular tetrahedron.

To further investigate the potential factors that influence the photocatalytic hydrogen evolution process, a tetrahedral analogue with the same structural features but an almost solid sphere was designed and prepared. The H_3**TCT** ligand, 2,2′,2″-(benzene-1,3,5-triyltris(methanylylidene))tris(hydra-zinecarbo-thioamide), was prepared via the reaction of thiosemicarbazide with benzene-1,3,5-tricarbaldehyde in a 3:1 mol ratio. The reaction of H_3**TCT** with $Co(CH_3COO)_2{\cdot}4H_2O$ in DMF produced Co-**TCT** in 42% yield. Elemental and powder X-ray analyses indicated the bulk sample consisted of a single pure phase. The ESI-MS spectrum of the Co-**TCT** complex in the solution exhibited $[Co_4(TCT)_4]^+$ peak at m/z = 1748.89, suggesting the formation of the similar M_4L_4 species in the solution. However, attempts to obtain signals relevant to the host−guest complexation species failed whenever various concentrations of **Fl** were added to the solution. Cyclic voltammetry of Co-**TCT** exhibited a broad peak at approximately −1.03 V (vs Ag/AgCl, Figure 5a) assignable to the coupled Co^{II}/Co^{I} and Co^{III}/Co^{II} processes. This potential is consistent with the Co-**TCT** tetrahedron and permits the exploration of redox-induced reactions near the H_2/H^+ couple.

Crystal structure analysis revealed that Co-**TCT** exhibits ideal T symmetry, with its cobalt ions and ligands located on the crystallographic C_3 axis (Scheme 2). Each cobalt center has the same coordination environment as those in Co-**TFT** (Supporting Information Figure S4). The average distance between cobalt ions was 10.18 Å. The separation between the center of the tetrahedron and the central points of the meta-substituted benzenes was approximately 3.37 Å, giving an inner volume of approximately 160 Å^3. The rhombus opening exhibited two diagonal lengths of 10.1 and 3.94 Å. Because the van der Waals radius of a monatomic molecule is approximately 3.6 Å, the sphere of Co-**TCT** was clearly almost solid and the size of the pocket was too small for an **Fl** molecule to be encapsulated.[60] Because Co-**TCT** and Co-**TFT** exhibited almost the same coordination structures and redox potentials, Co-**TCT** was considered an ideal reference compound for Co-**TFT** in the investigation of photocatalytic hydrogen evolution from water within a supramolecular system.

Scheme 2. Structures of the Molecular Tetrahedra of the Cobalt Ions and the Different Radii of the Pockets (red balls)[a]

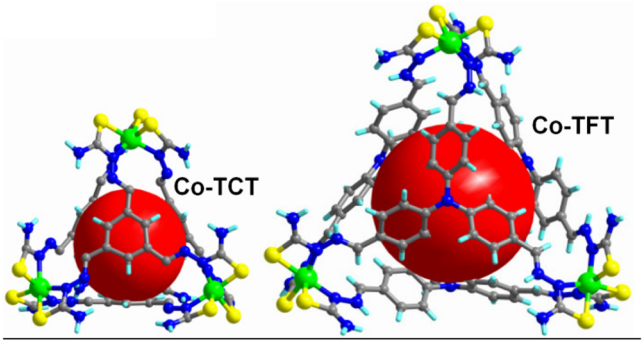

	Co–**TFT**	Co–**TCT**
Co–S in an average (Å)	2.30 (1)	2.20(1)
Co–N in an average (Å)	1.96(1)	1.93(6)
C(1)–S in an average (Å)	1.71(1)	1.70(2)
C(1)–N_{NH2} in an average (Å)	1.34(2)	1.33(2)
C(1)–N_{Imin} in an average (Å)	1.32(1)	1.30(1)
Co···Co in an average (Å)	15.58(5)	10.10(6)

[a]Cobalt, sulfur, nitrogen, and carbon atoms are drawn in green, yellow, blue, and gray, respectively.

The photolysis of a solution containing 0.2 mM **F1** and Co-**TCT** (10.0 μM) in a solvent mixture containing **NEt**$_3$ (10% in volume) and EtOH/H_2O (1:1 in volume) resulted in hydrogen generation under the photocatalytic conditions optimized at pH = 11.6. The TOF was approximately 450 mol of hydrogen per mole of catalyst per hour, and the TON was approximately 4500 mol of hydrogen per mole of redox catalyst (Figure 6b). The volume of the generated hydrogen was approximately 40% that produced by Co-**TFT** under the same experimental conditions and with an equal concentration of the redox catalyst. Experiments also showed that the addition of 2.0 mM ATP to the Co-**TCT**(10.0 μM)/**Fl**(2.0 mM)/**NEt**$_3$ system did not obviously affect hydrogen evolution (Figure 7a), demonstrating the normal homogeneous dynamics behavior of the system. Because the two tetrahedra exhibit almost exactly the same structural features and redox potentials, the superiority of the Co-**TFT**/**Fl**/**NEt**$_3$ systems over Co-**TCT**/**Fl**/**NEt**$_3$ is attributed to the well-emerged new reaction pathways of the Co-**TFT**/**Fl**/**NEt**$_3$ systems and the increased molarity of the reaction within the confined space.

The luminescence titration of **Fl** (10 μM) exhibited a quenching of approximately 38% of the luminescence intensity upon the addition of up to 50 μM Co-**TCT** (Supporting Information Figure S13). The decrease in the lifetime (from 4.5 to 4.0 ns) of **Fl** upon addition of Co-**TCT** (50 μM) confirmed a normal intermolecular quenching process (Figure 8a). Given

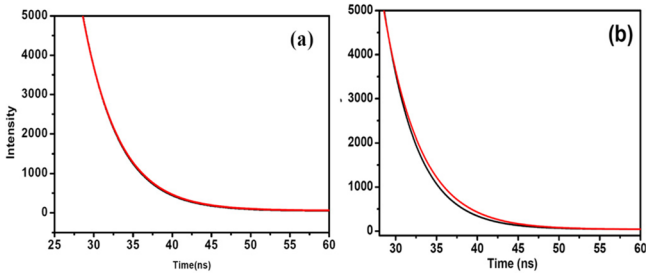

Figure 8. Luminescence decay of **Fl** (10.0 μM, red line) in EtOH/H_2O (1:1, pH = 11.6) and of the aforementioned solution upon addition of (a) Co-**TFT** (50.0 μM) or (b) Co-**TCT** (50.0 μM). The intensity was recorded at 525 nm; the excitation wavelength was 472.6 nm.

that the concentration of **NEt**$_3$ (10%, 0.72 M) was much higher than that of Co-**TCT** in the reaction mixture, a PET from the **NEt**$_3$ to the excited state of the organic dye (reduction quenching) dominated the homogeneous photolysis instead of direct quenching by Co-**TCT**. Meanwhile, the decrease in fluorescence lifetime of **Fl** (0.1 mM) upon the addition of 0.72 M **NEt**$_3$ (3.6 ns) confirmed that the PET process from **Et**$_3$**N** to the excited state **Fl*** dominated the photocatalytic processes. Notably, the direct quenching of the excited state **Fl*** by the molecular tetrahedron produced Fl^+ species and avoid the formation of unstable PS^- radical anions, thus prolonging the

DOI: 10.1021/jacs.5b00832
J. Am. Chem. Soc. 2015, 137, 3967−3974

lifetime of the system.[61] The well-emerged new PET pathway contributed to the superiority of the supramolecular system over normal homogeneous systems.

Whereas the cobalt ions exhibited uncommon coordination geometry, the preparation of a mononuclear cobalt complex containing a tristhiosemicarbazone moiety resembling the corner of the molecular tetrahedron as another reference material was rigorously pursued. The ligand H**DMT**, 2-(4-(dimethylamino) benzylidene) hydrazinecarbothioamide, was synthesized according to method described in the literature.[62] The cobalt complex Co-**DMT** was synthesized in approximately 66% yield by reacting $Co(CH_3COO)_2{\cdot}4H_2O$ with ligand H**DMT** with in DMF. Elemental analysis and powder X-ray analysis indicated that the bulk sample consisted of a single pure phase. Single-crystal structure analysis of revealed that the cobalt center was affixed to three sulfur atoms and three nitrogen atoms. These donors belonged to three bidentate chelators, two of which were five-membered rings and the other of which was a four-membered ring (Figure 9).

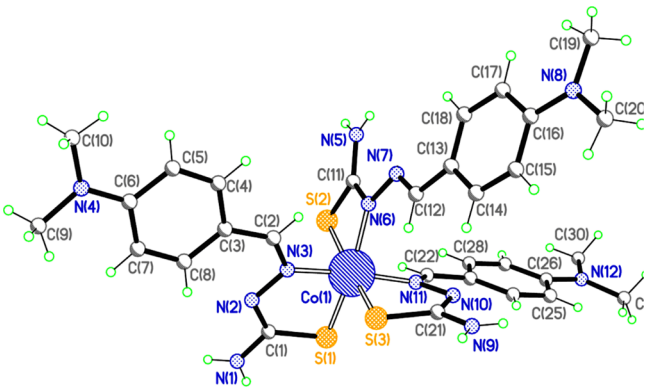

Figure 9. Molecular structure with the atomic-numbering scheme of Co-**DMT**.

The irradiation of a solution containing 0.2 mM **Fl** and Co-**DMT** (40.0 μM) in a solvent mixture containing $\mathbf{Et_3N}$ (10% in volume) and $EtOH/H_2O$ (1:1 in volume) resulted in hydrogen generation at pH = 11.6. Approximately 2.75 mL of hydrogen was produced after irradiating for 24 h, and the addition of ATP (2.0 mM) did not change the volume of hydrogen produced (Figure 7). In comparison to the 12.3 mL of hydrogen produced in the Co-**TFT**/**Fl**/$\mathbf{NEt_3}$ system under the same reaction conditions (10 μM of Co-**TFT**, ensuring the same concentration of cobalt ions), Co-**DMT** exhibited a considerably lower catalytic activity. The superiority of the Co-**TFT**/**Fl**/$\mathbf{NEt_3}$ system over the Co-**DMT**/**Fl**/$\mathbf{NEt_3}$ system is attributed to the new reaction pathways of the Co-**TFT**/**Fl**/$\mathbf{NEt_3}$ system and to the increased molarity of the reaction within the confined space. The luminescence titrations of **Fl** (10 μM) quenched approximately 35% of the emission upon the addition of up to 0.2 mM Co-**DMT**. The decrease in fluorescence lifetime (from 4.5 to 4.0 ns) of **Fl** (0.1 mM) upon the addition of Co-**DMT** (0.2 mM) confirmed that the PET occurred in a normal bimolecular manner. Because the decrease in fluorescence lifetime of **Fl** upon the addition of 0.72 M $\mathbf{NEt_3}$ (3.6 ns) is quite larger than that of Co-**DMT**, a reduction quenching by $\mathbf{NEt_3}$ clearly dominates the homogeneous photolysis rather than oxidative quenching by Co-**DMT**.

3. CONCLUSION

In summary, a new strategy for the construction of artificial photocatalytic systems for the generation of hydrogen from water by encapsulating an organic photosensitizer in the pocket of a redox metal−organic polyhedron was reported. Within the confined space, these essential components were forced closer together, and the pseudo-intramolecular PET from the excited state of the photosensitizer to the redox cobalt sites was modified to avoid unwanted electron-transfer processes. Control experiments based on the mononuclear compound and a smaller tetrahedral analogue with a solid sphere suggested that the superiority of the supramolecular systems over others was attributable to the well-elucidated new reaction pathways and to the increased molarity of the reaction within the confined space. New supramolecular artificial photocatalytic systems with improved efficiency were created by further modification of the structures and redox potentials of the metal−organic polyhedrons to match the electronic configuration and energy levels of the organic guests.

4. EXPERIMENTAL SECTION

4.1. Materials and Methods. All chemicals were of reagent-grade quality, were obtained from commercial sources, and were used without further purification. ^{1}H NMR spectra were measured on a Varian INOVA 400 and 100 M spectrometer. ESI-MS was carried out on an HPLC-Q-Tof mass spectrometer. The elemental analyses of C, H, and N were performed on a Vario EL III elemental analyzer. UV−vis spectra were measured on an HP 8453 spectrometer. The solution fluorescence spectra were measured on a JASCO FP-6500. The solution of fluorescein was prepared in $EtOH/H_2O$ 1:1 (v:v), whereas the solution of Co-**TFT** was prepared in DMF. The high-concentration stock solution of ATP (10.0 mM) was prepared directly in 9:1 DMF/H_2O (v:v). Electrochemical measurements were performed on a ZAHNER ENNIUM electrochemical workstation with a conventional three-electrode system consisted of a homemade Ag/AgCl electrode as the reference electrode, a piece of platinum silk 0.5 mM diameter as the counter electrode, and a glassy carbon electrode as the working electrode. The measurements were performed at room temperature after the solutions were degassed with nitrogen.

Photoinduced hydrogen evolution was carried out in a 40 mL flask. Various amounts of the catalyst, **Fl**, and $\mathbf{NEt_3}$ in 1:1 $EtOH/H_2O$ were added to obtain a total volume of 5.0 mL. The flask was sealed with a septum and degassed by bubbling nitrogen for 15 min under atmospheric pressure at room temperature. The pH of this solution was adjusted to a specific pH by adding H_2SO_4 or NaOH and was measured with a pH meter. The samples were subsequently irradiated by a 500 W xenon lamp. The reaction temperature was maintained at 293 K using a water filter to absorb heat. The generated photoproduct of H_2 was characterized using a GC 7890T gas chromatograph equipped with a 5 Å molecular sieve column (0.6 m × 3 mm) and a thermal conductivity detector; nitrogen was used as the carrier gas. The amount of hydrogen generated was determined by the external standard method. Hydrogen was not measured in the resulting solution, and the slight effect of the generated hydrogen gas on the pressure of the flask was neglected for the calculation of the volume of hydrogen gas.

4.2. Syntheses and Characterizations. *Preparation of H_3**TFT**.* 2,2′,2″-((Nitrilotris(benzene-4,1-diyl))tris(methanylylidene))tris-(hydrazinecarbothioamide): Five drops of acetic acid was added to a mixture of tris(4-formylphenyl) amine (0.33 g, 1.0 mmol) and thiosemicarbazine (0.27 g, 3.0 mmol) in a methanol solution. After the mixture was refluxed for 6 h, the yellow precipitate formed was collected by filtration, washed with methanol, and dried in vacuum. Yield: 85%. Anal. calcd for $C_{24}H_{24}N_{10}S_3{\cdot}H_2O$: H, 4.41; C, 52.53; N, 25.53. Found: H, 4.60; C, 52.10; N, 25.05. ^{1}H NMR (DMSO-d_6, ppm) δ 11.38 (s, 3H, NH), 8.15 (w, 3H, $-NH_2$), 8.01(s, 3H, CH═N), 7.91

DOI: 10.1021/jacs.5b00832
J. Am. Chem. Soc. 2015, 137, 3967−3974

(w, 3H, $-NH_2$), 7.76(d, 6H, phenyl), 7.06 (d, 6H, phenyl). ^{13}C NMR (DMSO-d_6, ppm) δ 178.5, 148.6, 146.5, 127.9, 124.8.

Preparation of ***Co-TFT***. H_3**TFT** (54.8 mg, 0.10 mmol) and $Co(CH_3COO)_2{\cdot}4H_2O$ (24.9 mg, 0.10 mmol) were dissolved in DMF (5 mL). After the solution was refluxed for 4 h, the reaction mixture was cooled to room temperature. Black crystals of Co-**TFT** were obtained by diffusing methanol into the aforementioned DMF solution. Yield: approximately 48% (based on the crystals dried under vacuum). Anal. calcd for $Co_4C_{96}H_{84}N_{40}S_{12}{\cdot}4C_3H_7NO$: H, 4.16; C, 47.85; N, 22.73; Found: H, 4.36; C 47.38; N 22.47. ^1H NMR (DMSO-d_6, ppm) 8.11 (s, 3H, CH═N), 7.78 (br, 6H, $-NH_2$), 7.26 (d, 3H, phenyl), 7.17 (d, 3H, phenyl), 6.38 (d, 3H, phenyl), 6.22(d, 3H, phenyl). ^{13}C NMR(DMSO-d_6, ppm); δ 163.5, 149.6, 148.5, 128.9, 125.8.

Preparation of H_3***TCT***. 2,2′,2″-(Benzene-1,3,5-triyltris (methanylylidene))tris(hydrazinecarbothio-amide): Five drops of acetic acid were added to a mixture of benzene-1,3,5-tricarbaldehyde (0.16 g, 1.0 mmol) and thiosemicarbazine (0.27 g, 3 mmol) in methanol solution, and the mixture was refluxed for 4 h. The yellow precipitate formed was collected by filtration, washed with methanol, and dried under vacuum. Yield: 90%. Anal. calcd for $C_{12}H_{15}N_9S_3{\cdot}2H_2O$: H, 4.59; C, 34.52.; N, 30.19. Found: H, 4.50; C, 34.64; N, 30.30. ^1H NMR (DMSO-d_6, ppm) δ 11.63 (s, 3H, NH), 8.30 (s, 3H, CH═N), 8.22 (s, 3H, phenyl), 8.08 (br, 6H, $-NH_2$). ^{13}C NMR (DMSO-d_6, ppm) δ: 178.6, 148.8, 134.1, 131.4.

*Preparation of Co-***TCT**. H_3**TCT** (38.1 mg, 0.10 mmol) and $Co(CH_3COO)_2{\cdot}4H_2O$ (24.9 mg, 0.10 mmol) were dissolved in DMF (10 mL). After the solution was refluxed for 4 h, the reaction mixture was cooled to room temperature. Black crystals of Co-**TCT** were obtained by diffusing methanol into the aforementioned DMF solution. Yield: approximately 42%. Anal. calcd for $Co_4C_{48}H_{48}N_{36}S_{12}$: H, 2.77; C, 32.95; N, 28.82; Found: H, 2.84; C 33.16; N 28.62. ^1H NMR (DMSO-d_6, ppm) 8.03(s, 3H, CH═N), 7.87 (br, 6H, $-NH_2$), 7.22(br, 3H, phenyl). ESI-Ms, M^+: 1748.89. ^{13}C NMR (DMSO-d_6, ppm); δ 163.6, 147.6, 133.2, 130.6.

*Preparation of Co-***DMF**. 2-(4(Dimethylamino)benzylidene)-hydrazinecarbothio-amide (H**DMT**, 22.2 mg, 0.1 mmol) and Co-$(CH_3COO)_2{\cdot}4H_2O$ (9.0 mg, 0.35 mmol) were dissolved in DMF (10 mL) and stirred overnight at room temperature. Black crystals of Co-**DMT** were obtained by diffusing ether into the DMF solution. Yield: approximately 66%. Anal. calcd for $CoC_{30}H_{39}N_{12}S_3$: H, 5.44; C, 49.85; N, 23.25; Found: H, 5.90; C 49.62; N 22.88. ESI-MS, M^+:723.19.

4.3. Crystallography. The intensities were collected on a Bruker SMART APEX CCD diffractometer equipped with a graphite-monochromated Mo−Kα (λ = 0.71073 Å) radiation source; the data were acquired using the SMART and SAINT programs.[63,64] The structures were solved by direct methods and refined on F^2 by full-matrix least-squares methods using the SHELXTL version 5.1 software.[65]

*Crystal Data for Co-***TFT**. $Co_4C_{134}H_{179}N_{52}O_{15.50}S_{12}$ M_r = 3386.73, rhombohedral, space group *R*-3*c*, dark-red block, a = 24.741(1) Å, c = 109.349(6) Å, V = 57967(5) Å^3, Z = 12, Dc = 1.164 g cm^{-3}, μ(Mo−Kα) = 0.530 mm^{-1}, T = 200(2)K. 11,347 unique reflections [R_{int} = 0.0846]. Final R_1 [with $I > 2\sigma(I)$] = 0.0735, wR_2 (all data) = 0.2339. CCDC no. 973241.

*Crystal Data for Co-***TCT**. $Co_4C_{40}H_{50}N_{40}O_8S_{12}$ M_r = 2079.84, cubic, space group *I*-43*m*, dark-red block, a = 20.884(1) Å, V = 9108.9 (6) Å^3, Z = 2, μ(Mo−Kα) = 0.531 mm^{-1}, T = 200(2) K. 1439 unique reflections [R_{int} = 0.1088]. Final R_1 [with $I > 2\sigma(I)$] = 0.0670, wR_2 (all data) = 0.1615. CCDC no. 1000791.

*Crystal Data for Co-***DMT**. $CoC_{42}H_{67}N_{16}O_4S_3$, M_r = 1015.23, monoclinic, space group $P2_1/c$, dark-red block, a = 9.712(1),b = 24.697(2), c = 21.697(2) Å, V = 5195.9(7) Å^3, Z = 4, Dc = 1.299 g cm^{-3}, μ(Mo−Kα) = 0.506 mm^{-1}, T = 296(2) K. 8094 unique reflections [R_{int} = 0.0939]. Final R_1 [with $I > 2\sigma(I)$] = 0.0787, wR_2 (all data) = 0.2005. CCDC no. 1000792.

*For Crystal Data of Co-***TFT**. Except for methanol (solvent) and water molecules, the other non-hydrogen atoms were refined anisotropically. The hydrogen atoms within the ligand backbones and the DMF molecules were fixed geometrically at calculated distances and allowed to ride on the parent non-hydrogen atoms. Several bond distances in two of the DMF molecules were constrained at ideal values, and the thermal parameters of adjacent atoms in these molecules were constrained to be similar.

*For Crystal Data of Co-***TCT**. The non-hydrogen atoms were refined anisotropically. The hydrogen atoms within the ligand backbones and the DMF molecules were fixed geometrically at calculated distances and allowed to ride on the parent non-hydrogen atoms. Two nitrogen atoms, the carbon atom, and the sulfur atom of the thiourea moiety were disordered into two parts with each S. O. F. fixed as 0.25; the corresponding bond distance in the two disordered parts were constrained at the same value. Several bond distances in the DMF molecules were constrained at ideal values, and the thermal parameters of adjacent atoms in these molecules were constrained to be similar.

*For Crystal Data of Co-***DMT**. The non-hydrogen atoms were refined anisotropically. The hydrogen atoms within the ligand backbones and the DMF molecules were fixed geometrically at calculated distances and allowed to ride on the parent non-hydrogen atoms. Three carbon atoms on one of the DMF molecules were disordered into two parts, and their S. O. F. was refined with free variables; the thermal parameters on adjacent atoms in the disordered DMF molecules were constrained to be similar.

■ ASSOCIATED CONTENT

Ⓢ Supporting Information

Crystal data (CIF file), experimental details, tables, and figures. This material is available free of charge via the Internet at http://pubs.acs.org.

■ AUTHOR INFORMATION

Corresponding Author

*E-mail: cyduan@dlut.edu.cn

Notes

The authors declare no competing financial interest.

■ ACKNOWLEDGMENTS

This work was supported by the National Natural Science Foundation of China (21421005 and 21231003) and the Basic Research Program of China (2013CB733700) and the Program for Changjiang Scholars and Innovative Research Team in University (IRT1213).

■ REFERENCES

(1) Kirby, A. J.; Hollfelder, F. *From Enzyme Models to Model Enzymes*; RSC Publishing: Cambridge, 2002.
(2) Lehn, J. M. *Science* **2002**, *295*, 2400−2403.
(3) Pauling, L. *Nature* **1948**, *161*, 707−709.
(4) Tabushi, I. *Acc. Chem. Res.* **1982**, *15*, 66−72.
(5) Yoshizawa, M.; Tamura, M.; Fujita, M. *Science* **2006**, *312*, 251−254.
(6) Oluth, M. D.; Bergman, R. G.; Raymond, K. N. *Science* **2007**, *316*, 85−88.
(7) Yoshizawa, M.; Klosterman, J. K.; Fijuta, M. *Angew. Chem., Int. Ed.* **2009**, *48*, 3408−3438.
(8) Loner, A. L.; Marquez, C.; Dickman, M. H.; Nau, W. M. *Agnew. Chem. Int. Ed.* **2011**, *50*, 545−548.
(9) Lee, J. W.; Samal, S.; Selvapalam, N.; Kim, H. J.; Kim, K. *Acc. Chem. Res.* **2003**, *36*, 621−630.
(10) Raynal, M.; Ballester, P.; Vidal-Ferran, A.; Leeuwen, P. W. N. M. *Chem. Soc. Rev.* **2014**, *43*, 1660−1733.
(11) Raynal, M.; Ballester, P.; Vidal-Ferran, A.; Leeuwen, P. W. N. M. *Chem. Soc. Rev.* **2014**, *43*, 1734−1787.
(12) Mahata, K.; Frischmann, P. D.; Würthner, F. *J. Am. Chem. Soc.* **2013**, *35*, 15656−15661.
(13) Furutani, Y.; Kandori, H.; Kawano, M.; Nakabayashi, K.; Yoshizawa, M.; Fujita, M. *J. Am. Chem. Soc.* **2009**, *131*, 4764−4768.
(14) Gray, H. B.; Maverick, A. W. *Science* **1981**, *214*, 1201−1205.

DOI: 10.1021/jacs.5b00832
J. Am. Chem. Soc. 2015, 137, 3967−3974

(15) Lewis, N. S.; Nocera, D. G. *Proc. Natl. Acad. Sci. U.S.A.* **2006**, *103*, 15729−15735.
(16) Esswein, A. J.; Nocera, D. G. *Chem. Rev.* **2007**, *107*, 4022−4047.
(17) Wang, J.; He, C.; Wu, P. Y.; Wang, J.; Duan, C. Y. *J. Am. Chem. Soc.* **2011**, *133*, 12402−12405.
(18) Porel, M.; Chuang, C. H.; Burda, C.; Ramamurthy, V. *J. Am. Chem. Soc.* **2012**, *134*, 14718−14721.
(19) Kitamoto, K.; Sakai, K. *Angew. Chem., Int. Ed.* **2014**, *53*, 4618−4622.
(20) Frischmann, P. D.; Mahata, K.; Würthner, F. *Chem. Soc. Rev.* **2013**, *42*, 1847−1870.
(21) Chakrabarty, R.; Mukherjee, P. S.; Peter J. Stang, P. J. *Chem. Rev.* **2011**, *111*, 6810−6918.
(22) Leininger, S.; Olenyuk, B.; Stang, P. J. *Chem. Rev.* **2000**, *100*, 853−907.
(23) Seidel, S. R.; Stang, P. J. *Acc. Chem. Res.* **2002**, *35*, 972−983.
(24) Stang, P. J.; Olenyuk, B. *Acc. Chem. Res.* **1997**, *30*, 502−518.
(25) Debata, N. B.; Tripathy, D.; Chand, D. K. *Coord. Chem. Rev.* **2012**, *256*, 1831−1945.
(26) Smulders, M. M. J.; Riddell, I. A.; Browne, C.; Nitschke, J. R. *Chem. Soc. Rev.* **2013**, *42*, 1728−1754.
(27) Wiester, M. J.; Ulmann, P. A.; Mirkin, C. A. *Angew. Chem., Int. Ed.* **2011**, *50*, 114−137.
(28) Meeuwissen, J.; Reek, J. N. H. *Nat. Chem.* **2010**, *2*, 615−621.
(29) Wang, Z. J.; Clary, K. N.; Bergman, R. G.; Raymond, K. N.; Toste, F. D. *Nat. Chem.* **2013**, *5*, 100−103.
(30) He, Q. T.; Li, X. P.; Lu, Y.; Yu, Z. Q.; Wang, W.; Su, C. Y. *Angew. Chem., Int. Ed.* **2009**, *48*, 6156−6159.
(31) Vriezema, D. M.; Aragonès, M. C.; Elemans, J. A. A. W.; Cornelissen, J. J. L. M.; Rowan, A. E.; Nolte, R. J. M. *Chem. Rev.* **2005**, *105*, 1445−1489.
(32) Wang, Z. J.; Clary, K. N.; Bergman, R. G.; Raymond, K. N.; Toste, F. D. *Nat. Chem.* **2013**, *5*, 100−103.
(33) Inokuma, Y.; Kawano, M.; Fujita, M. *Nat. Chem.* **2011**, *3*, 349−358.
(34) Bolliger, J. L.; Belenguer, A. M.; Nitschke, J. R. *Angew. Chem., Int. Ed.* **2013**, *52*, 7958−7962.
(35) Zarkadoulas, A.; Koutsouri, E.; Mitsopoulou, C. A. *Coord. Chem. Rev.* **2012**, *256*, 2424−2434.
(36) McNamara, R. W.; Han, Z. J.; Yin, C. J.; Brennessel, W. W.; Holland, P. L.; Eisenberg, R. *Proc. Natl. Acad. Sci. U.S.A.* **2012**, *109*, 15595−15599.
(37) Konigstein, C. A. *J. Photochem. Photobiol.* **1995**, *90*, 141−152.
(38) Na, Y.; Pan, J. X.; Wang, M.; Sun, L. C. *Inorg. Chem.* **2007**, *46*, 3813−3815.
(39) Paterson, B. M.; White, J. M.; Donnelly, P. S. *Dalton Trans.* **2010**, *39*, 2831−2837.
(40) Viñuelas-Zahínos, E.; Luna-Giles, F.; Torres-García, P.; Fernández- Calderón, M. C. *Eur. J. Med. Chem.* **2011**, *46*, 150−159.
(41) Zhao, Y. G.; Guo, D.; Liu, Y.; He, C.; Duan, C. Y. *Chem. Commun.* **2008**, 5725−5727.
(42) Li, M. X.; Cai, P.; Duan, C. Y.; Lu, F.; Xie, J.; Meng, Q. J. *Inorg. Chem.* **2004**, *43*, 5174−5176.
(43) Zhang, T.; Liu, G. F.; Liu, L.; Jia, D. Z.; Zhang, L. *Chem. Phys. Lett.* **2006**, *427*, 443−448.
(44) Chang, T. M.; Tomat, E. *Dalton Trans.* **2013**, *42*, 7846−7849.
(45) Lazarides, T.; McCormick, T. M.; Du, P. W.; Luo, G. G.; Lindley, B.; Eisenberg, R. *J. Am. Chem. Soc.* **2009**, *131*, 9192−9194.
(46) Zhang, P.; Wang, M.; Dong, J. F.; Li, X. W.; Wang, F.; Wu, L. Z.; Sun, L. C. *J. Phys. Chem. C* **2010**, *114*, 15868−15874.
(47) Dong, J. F.; Wang, M.; Zhang, P.; Yang, S. Q.; Liu, J. Y.; Li, X.; Sun, L. C. *J. Phys. Chem. C* **2011**, *115*, 15089−15096.
(48) McCormick, T. M.; Han, Z. J.; Weinberg, D. J.; Brennessel, W. W.; Holland, P. L.; Eisenberg, R. *Inorg. Chem.* **2011**, *50*, 10660−10666.
(49) Biros, S. M.; Yeh, R. M.; Raymond, K. N. *Angew. Chem., Int. Ed.* **2008**, *47*, 6062−6064.
(50) Baffert, C.; Artero, V.; Fontecave, M. *Inorg. Chem.* **2007**, *46*, 1817−1824.
(51) Artero, V.; Chavarot-Kerlidou, M.; Fontecave, M. *Angew. Chem., Int. Ed.* **2011**, *50*, 7238−7266.
(52) Jiang, P. J.; Guo, Z. J. *Coord. Chem. Rev.* **2004**, *248*, 205−229.
(53) Connors, K. A. *Binding Constants*; John Wiley: New York, 1987.
(54) Nelissen, H. F. M.; Kercher, M.; De Cola, L.; Feiters, M. C.; Nolte, R. J. M. *Chem.—Eur. J.* **2002**, *8*, 5407−5414.
(55) Zhang, P.; Wang, P.; Na, Y.; Li, X. Q.; Jiang, Y.; Sun, L. C. *Dalton Trans.* **2010**, *39*, 1204−1206.
(56) Yamade, Y.; Miyahigashi, T.; Kotani, H.; Ohkubo, K.; Fukuzumi, S. *J. Am. Chem. Soc.* **2011**, *133*, 16136−16145.
(57) McCormick, T. M.; Calitree, B. D.; Orchard, A.; Kraut, N. D.; Bright, F. V.; Detty, M. R.; Eisenberg, R. *J. Am. Chem. Soc.* **2010**, *132*, 15480−15483.
(58) He, C.; Wang, J.; Zhao, L.; Liu, T.; Zhang, J.; Duan, C. Y. *Chem. Commun.* **2013**, *49*, 627−629.
(59) McKee, T.; McKee, J. R. *Biochemistry: The Molecular Basis of Life*, 3rd ed.; McGraw-Hill: New York, 2003.
(60) Liu, Y.; Lin, Z. H.; He, C.; Zhao, L.; Duan, C. Y. *Dalton Trans.* **2010**, *39*, 11122−11125.
(61) Han, Z.; McNamara, W. R.; Eum, M. S.; Holland, P. L.; Eisenberg, R. *Angew. Chem., Int. Ed.* **2012**, *51*, 1667−1670.
(62) Sampath, N.; Mathews, R.; Ponnuswamy, M. N.; Kang, L. *Mol. Cryst. Liq. Cryst.* **2010**, *518*, 151−159.
(63) *SMART Data collection software*, version 5.629; Bruker AXS Inc.: Madison, WI, 2003.
(64) *SAINT, Data reduction software*, version 6.45 Bruker AXS Inc.: Madison, WI, 2003.
(65) Sheldrick, G. M. *SHELX-97: Program for crystal structure analysis*; University of Göttingen: Göttingen, Germany, 1997.

DOI: 10.1021/jacs.5b00832
J. Am. Chem. Soc. 2015, 137, 3967−3974